Research Article

Performance Analysis of a Novel Compressed Carbon Dioxide Storage Model Integrated with Solar Energy

Samira Jafari, Mehran Ameri *

Department of Mechanical Engineering, School of Engineering, University of Shahid Bahonar, P. O. Box: 76175-133, Kerman, Kerman, Iran.

ABSTRACT

As a result of growing energy demand, shortage of fossil fuel resources, climate change, and environmental protection, the need for renewable energy sources has been growing rapidly. However, there is an urgent need to cope with intermittency and fluctuation of renewable energies. Various energy storage systems are considered as appropriate solutions to the above-mentioned problem. In the present manuscript, a novel compressed carbon dioxide energy storage system was proposed. Furthermore, an extra thermal energy storage with Therminol VP-1 as a working fluid, coupled with Parabolic Trough Collector (PTC), was added to the system. This integration is conducive to rising the inlet temperature of turbines and reducing the work load that should be done by the compressors. In the present study, a method based on software product including Engineering Equation Solver (EES) for determining thermodynamic characters per component and System Advisor Model (SAM) was employed to model the solar field for a desired location. Energy and exergy analyses were conducted to evaluate the whole cycle performance during charging and discharging periods. In this study, the city of Kerman located in the south-eastern part of Iran, with Direct Normal Incidence (DNI) of 950 $\frac{W}{m^2}$, was selected for the present modeling. The results of a random day (June 22/2019) at time 15:00 represented the exergy efficiency of 66.98 % and the round trip efficiency of 93.14 %. High exergy efficiency and round trip efficiency of this system make this idea applicable to enhancing the total performance of the entire system.

1. INTRODUCTION

In recent years, much attentions has been given to renewable energy sources such as solar photovoltaic, wind, geothermal, biofuel, biomass, tidal, etc. as a result of two major concerns including climate change and energy security.

It should be kept in mind that these renewable energy sources are subject to a major drawback, namely intermittent and fluctuating nature. As a reasonable solution to the above-mentioned problem, various methods have been proposed. Energy storage process includes changing the form of available electricity to another, which can again be converted easily to electricity. A proper energy storage method can be used to make a balance between electricity supply and demand. Moreover, energy storage methods can guarantee grid stability and security. There are diverse methods such as pumped-hydro, compressed air, liquid air, and compressed carbon dioxide to store energy.

Pumped Hydro Energy Storage (PHES) method is among the most common energy storage technologies as a result of its large-scale capacity and economic benefits [1]. PHES method employs cheap electricity during off-peak hours to pump water from a smaller source to a larger one. On the contrary, during peak hours, the water gathered in the larger source is

freed in order to activate hydro turbine and generate electricity. The energy efficiency of the installed PHES plants worldwide has been reported to be between 70 % and 80 % with capacities of 1000-1500 MW, in order. It should be noted that this method suffers topography and geology constraints as a major difficulty. In other words, a typical pumped hydro energy storage system acquires sufficient elevation difference between its reservoirs. Owing to the low energy density of pumped hydro energy storage, this technology needs either a large amount of water or a noticeable height difference between sources [2].

Another large-scale thermal energy storage method is Compressed Air Energy Storage (CAES) method. In comparison with PHES method, CAES-based technologies are independent of massive amount of water and significant height difference between the reservoirs [3]. The initial notion behind using compressed air for energy storage was suggested by Gay in 1948 in a patent [4]. Following the excessive demand for energy in the last decades of 1960, CAES becomes more practical [5]. CAES method has two principal sub-categories: Diabatic CAES (D-CAES) and Adiabatic CAES (A-CAES).

In the case of D-CAES method, when the demand is low, the entrance air is compressed and fed into the ground tanks or underground cavities. Subsequently, when the demand is high, the air gathered in the cavities is drawn up using excess

*Corresponding Author's Email: ameri_mm@mail.uk.ac.ir (M. Ameri)
URL: https://www.jree.ir/article_137352.html

electricity and, afterwards, its temperature increases through natural gas in the combustion chamber. Then, the gas is expanded in the turbine to produce electric power. As previously described, the effect of greenhouse gases can be observed in the case of D-CAES method as a result of combustion process. In order to resolve this problem, A-CAES method has been proposed. In this method, a central thermal storage unit is used as a substitute for pre-coolers and post-heaters in the compressed air energy storage method [6].

In A-CAES procedure, whilst there is excess electricity available, the air is compressed. Then, the air goes across the thermal storage unit and eventually it is kept in the reservoir which can be located under the ground or over it. In case of high demand, the compressed air collected in the reservoir is drawn up to the thermal storage unit to be heated again. Thereafter, it goes across the turbine to generate electricity. A-CAES reduces the need for combustion chamber. The theoretical efficiency of this method was reported to be 70 % [6].

Both of the previously described compressed air-based energy storage methods require large cavities whether under or above the ground to store compressed air. In order to resolve this difficulty, researchers are interested in using liquid air as a storage medium [3].

In the process of Liquid Air Energy Storage (LAES), in addition to heat recovery and heat storage due to the compression process, the capacity of cold energy storage has been used to liquefy the air for storage [5].

During the discharge period, the liquid air is extracted from storage tanks and is pumped to higher pressure. Afterwards, the air is evaporated to the superheated state and eventually, it leads to production of high pressure gas can be used for operating turbines and generating electric power [7].

In 1997, Smith [8] was the first who suggested that recovery of cold energy from liquid air for use in the liquefaction process can enhance the storage efficiency. Although this method is characterized by some advantages including reducing the volume of compressed air and increasing the energy storage capacity [5], it is subject to some drawbacks including the need for a significantly low critical temperature which increases the need for precise insulation. Moreover, liquid air and its vapor can rapidly freeze body tissue and make many materials brittle [3].

Recently, integration of energy storage systems with carbon dioxide as the working fluid is one of the newest and most reliable methods for designing thermo-electric energy storage systems. Table (1) represents the thermo physical properties of carbon dioxide as working fluid [9].

Table 1. Thermo-physical properties of carbon dioxide [9]

Fluid name	ASHRAE No. Level for safety	Critical temperature (ºC) Pressure (Bar)	ODP	GWP 100yr	ds/dT
Carbon dioxide	R744 A1	30.98 73.8	0	1	-8.27

According to Table (1), carbon dioxide is a natural, environmentally benign refrigerant. What's more, its Global Warming Potential (GWP) is low and its Ozone Depleting Potential (ODP) indicates zero result. In addition, carbon dioxide is an inexpensive, non-explosive and cost-effective option [10]. The aforementioned reasons make carbon dioxide

an acceptable choice as a working fluid. New researches have focused on using carbon dioxide as a storage medium [11].

Mercangoz et al. [12] in 2012 suggested a carbon dioxide power cycle coupled with an electrical energy storage system. In their study, hot water and ice were used as storage materials. They concluded that the efficiency of this method was higher than that of the compressed air energy storage method and lower than that of the pumped hydro energy storage method.

Thereafter, Wang et al. [3] in 2015 presented a storage method based on liquid compressed air carbon dioxide. Their new system included high and low temperature storage units. Moreover, an additional organic Rankine cycle was designed to take full advantage of waste heat. Their results demonstrated that in comparison with the compressed air energy storage, their method exhibited higher energy generated per unit volume (EVR) and its efficiency could reach 56-64 %.

In 2016, to ensure the enhancement of energy storage density, Liu et al. [13] designed a storage system containing two saline aquifers as storage media in a close cycle for storing energy. They conducted energy and exergy analysis for the cycle. The exergy efficiency was reported to be 51.56 % for the supercritical carbon dioxide and 53.02 % for the transcritical carbon dioxide.

In 2019, Liu et al. [14] discussed conventional and advanced exergy analyses for a two-stage transcritical compressed carbon dioxide energy storage system. Their conclusion exhibited that the exergy efficiency of the cycle could reach up to 59 %.

In 2020, Yuan Zhang et al. [17] proposed an integrated system including transcritical carbon dioxide energy storage and Organic Rankine Cycle (ORC). They employed advanced exergy methods to optimize the performance of the entire cycle. They reported the exergy efficiency to be 34.62 %.

Later on, in 2020, Yuan Zhang et al. [1] presented a carbon dioxide storage method with low-temperature thermal storage in order to restore the heat in the compression process. In their research, in addition to parametric analysis, they used genetic algorithm to optimize key parameters. Finally, the round-trip efficiency, exergy efficiency, and thermal efficiency of this method were reported to be 41.4 %, 45.4 %, and 59.7 %, respectively.

Thereafter, Yuan Zhang et al. [18] in 2021 carried out conventional and advanced exergy analyses on the compressed carbon dioxide energy storage system and compressed air energy storage system under low-temperature conditions. They measured the exergy efficiency of compressed carbon dioxide as 56.28 % and 63.93 % for the similar compressed air energy storage.

Subsequently, Yuan Zhang et al. [19] in 2021 analyzed thermodynamic features of a compressed carbon dioxide energy storage system including carbon dioxide Brayton cycle, low-temperature thermal energy storage, and cold energy storage. They reported the exergy efficiency at 55.3 % under real conditions.

There are two commercial plants including Huntorf plant of 290 MW in Germany (1978) and McIntosh plant of 110 MW in America (1991). These plants operate based on compressed air energy storage [13]. In these plants, in the charging step, the heat produced from the compression process is released directly to the environment and the cooled compressed air is stored in a massive salt cavern. Furthermore, natural gas is employed to heat the compressed air in the discharging

process. For the above-stated reasons, the total system efficiency of these plants is recorded to be low (e.g., Huntorf plant efficiency is 42 % and McIntosh plant efficiency is 54 %). These operations yield an increase in the emission of carbon dioxide [13].

In order to achieve higher efficiency and energy storage density, attempts have been made in the form of suggestions to use carbon dioxide as the working fluid due to its greater density which causes a smaller volume for storage tank, compared to the compressed air. At the same time, employing solar power in place of natural gas during discharging step eliminate the carbon dioxide emission.

In the present paper, a combination of compressed carbon dioxide power cycle and concentrating solar power plant has been employed to generate and store electrical energy simultaneously. The novelty of the present study lies in the employment of a parabolic trough collector with the intention of supplying the energy required for preheating the entrance working fluid of the turbines. This approach leads to the enhancement of turbines' output power. Furthermore, in the current investigation, supercritical compressed carbon dioxide is used as liquid carbon dioxide with lower performance efficiency employed in similar conducted studies. This research is structured as in the following. First, the methodology employed in this article is discussed. Then, the schematic of the proposed cycle, its components, and its performance are introduced. Next, the thermodynamic modeling is introduced. Later, exergy analysis is presented. Eventually, the results are carried out in the last part.

2. METHOD

2.1. Methodology

In the present study, integration of software-based and manual calculations was employed to model the proposed cycle. Engineering Equation Solver (EES) was opted due to its thermodynamic database of high accuracy to model individual components. Since the open-source System Advisor Model (SAM) software is capable of analyzing concentrating solar power systems including parabolic trough, it has been selected for the present modeling. SAM software requires a weather data TMY file to begin the modeling process for a desired location. Afterwards, design point parameters should be specified. Then, solar field parameters including collectors, receivers, and thermal storage systems must be determined. Eventually, by means of the aforementioned data, the modeling can be completed.

2.2. Description of proposed system

A schematic of the proposed system is given in Figure (1). The main components of this system can be addressed as Compressors 1 & 2, Turbines 1 & 2, Coolers 1 & 2, Heaters 1, 2 & 3, Throttle valves 1 & 2, High-pressure carbon dioxide storage tank, Low-pressure carbon dioxide storage tank, Cold water tank, Hot water tank, Hot TV-oil tank, Cold TV-oil tank, Parabolic Trough collector, and Pump.

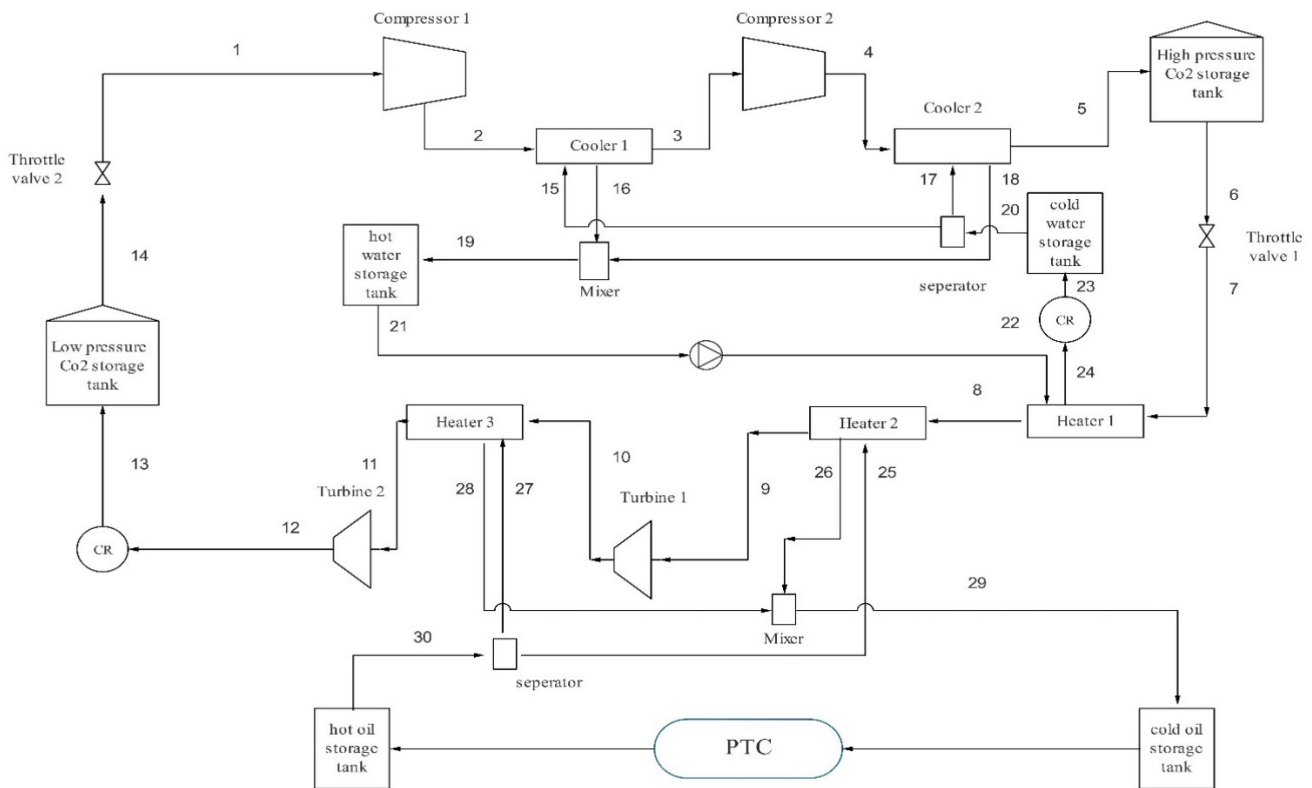The performance of this cycle is divided into charging and discharging processes.

Figure 1. Schematic of the proposed system

2.2.1. Charging process

During off-peak hours, carbon dioxide is compressed by means of excess energy in hand. Then, compressed carbon dioxide is stored in a high-pressure storage tank. The details of this process are described below:

Stream 14: This stream contains low-pressure liquid carbon dioxide (1 Mpa), which is extracted from the low-pressure carbon dioxide storage tank.

Stream 1: This stream is the outlet stream of throttle valve 2 whose pressure has been reduced to 0.7 Mpa. Then, it goes into Compressor 1.

Stream 2: The compressed carbon dioxide exits Compressor 1 in Stream 2. Meanwhile, the temperature of carbon dioxide decreases by means of cold water (Stream 15) through Cooler 1.

Stream 3: It is the outlet of Compressor 1 whose temperature is set to be 313.15 K to keep it supercritical.

Stream 4: It is the outlet of Compressor 2 whose temperature similarly decreases via cold water (Stream 17).

Stream 5: It is the exiting stream of Compressor 2 whose temperature is 313.15 K and its pressure is 20 Mpa and it approaches the high-pressure carbon dioxide tank.

2.2.2. Discharging process

During peak hours, the stored compressed carbon dioxide is used to activate turbines to generate electricity.

Stream 6: It is the outlet stream of the high-pressure carbon dioxide storage tank.

Stream 7: The temperature and pressure of Stream 6 after passing through throttle valve 1 are reduced. Next, it goes through Heater 1 whose temperature increases by means of hot water (Stream 22) which is recovered from the hot water tank.

Stream 8: It is the exiting stream of Heater 1 fed into Heater 2.

Stream 9: It is the outlet stream of Heater 2 whose temperature increases by means of hot oil stream (Stream 25).

Stream 10: It is the exiting stream of Turbine 1 which goes to Heater 3 and its temperature rises via hot oil stream 27 in the same manner.

Stream 11: It is the outlet stream of Heater 3 which goes to Turbine 2.

Stream 12: This stream exchange heat with a massive amount of air creates an environment where its temperature reaches ambient temperature.

Stream 13: It is the outlet stream of cooler which is stored in a low-pressure carbon dioxide tank storage.

3. PERFORMANCE ANALYSIS METHOD

This section includes thermodynamic modeling. First, the assumption used in this modeling were introduced. Subsequently, energy analysis containing individual component role and modeling is discussed. At last, exergy analysis is investigated.

3.1. Assumptions

The following assumptions are taken into account in order to simulate the proposed cycle in this article [14].

1) A constant isentropic efficiency value is set for compressors, turbines, and heat exchangers.
2) The heat exchange between system components and environment is ignored.
3) The pressure loss in pipes is neglected.
4) The pressure loss in heat exchangers is set to 0.02 Mpa.

3.2. Energy analysis

According to the first law of thermodynamics, energy balance can be written as in Eq. (1):

$$\dot{Q} - \dot{W} + \sum_i \dot{m}_i h_i - \sum_o \dot{m}_o h_o = 0 \tag{1}$$

In Eq. 1, $\dot{Q}$ represents net heat input, $\dot{W}$ is net power output, $\dot{m}$ is the mass flow rate, and h is the specific enthalpy. It

should be noted that subscripts i and o refer to inlet and outlet stream, respectively [15].

In this study, a two-stage compression and expansion cycle is employed. Throughout the proceeding sections, individual components will be discussed.

3.2.1. Compressor model

During the charging process, the input power of each compressor is derived from Eq. (2):

$$\dot{w}_{c_1} = \dot{m}_1(h_2 - h_1)$$

$$\dot{w}_{c_2} = \dot{m}_3(h_4 - h_3) \tag{2}$$

where w is input power, $\dot{m}$ is mass flow rate of carbon dioxide, subscripts c_1 and c_2 stand for Compressors 1 and 2 in Figure (1), and subscripts 1, 2, 3, and 4 denote the streams depicted in Figure (1) [1].

The isentropic efficiency of the compressors can be calculated using Eq. (3):

$$\eta_{c_1} = \frac{(h_{2,is} - h_1)}{(h_2 - h_1)}$$

$$\eta_{c_2} = \frac{(h_{4,is} - h_3)}{(h_4 - h_3)} \tag{3}$$

In the aforementioned equation, subscripts is stands for the isentropic process [1].

3.2.2. Turbine model

During the discharging process, the outlet power of each turbine can be calculated by Eq. (4):

$$\dot{w}_{T_1} = \dot{m}_9(h_9 - h_{10})$$

$$\dot{w}_{T_2} = \dot{m}_{12}(h_{11} - h_{12}) \tag{4}$$

where subscripts T_1 and T_2 stand for the turbines depicted in Figure (1) and subscripts 9, 10, 11, and 12 denote the streams shown in Figure (1) [1].

The isentropic efficiency of turbines can be driven from Eq. (5):

$$\eta_{T_1} = \frac{(h_9 - h_{10})}{(h_9 - h_{10,is})}$$

$$\eta_{T_2} = \frac{(h_{11} - h_{12})}{(h_{11} - h_{12,is})} \tag{5}$$

Subscripts is refers to the isentropic process [1].

3.2.3. Throttle valve model

Since the throttling process is isentropic, Eq. (6) is valid for modeling throttle valves:

$$h_7 = h_6$$

$$h_1 = h_{14} \tag{6}$$

Subscripts 1, 6, 7, and 14 are in line with the streams represented in Figure (1) [14].

3.2.4. CR model

CR functions like an after cooler in this cycle. As it is discussed previously in the literature, it is assumed that in this step, the working fluid and carbon dioxide exchange heat with plenty of air to reach the environment temperature [15]. Therefore, carbon dioxide condenses in gaseous state. Then, it can be stored in a low-pressure storage tank.

3.2.5. High-pressure and low-pressure carbon dioxide tank model

The state variation of carbon dioxide as a working fluid has not been considered during charging and discharging process in this study. Therefore, the inlet and outlet conditions do not vary in Eq. (7).

$$h_6 = h_5$$
$$h_{14} = h_{13} \tag{7}$$

where subscripts 5, 6, 13, and 14 are related to streams shown in Figure (1) [14].

Based on the assumptions made about storage tanks and throttle valves, only inlet conditions of storage tank and outlet conditions of the valve should be taken into account. The pressure and temperature difference can be calculated through Eq. (8).

$$P_7 = P_5 - \Delta P_{5-7}$$
$$T_7 = T_5 - \Delta T_{5-7} \tag{8}$$

where P refers to pressure, T denotes temperature, ΔP_{5-7} refers to pressure difference between States 5 and 7, and ΔT_{5-7} denotes temperature difference between States 5 and 7 [15].

3.2.6. Cooler and heater model

The heat exchange rate in heat exchangers shown in Figure (1) can be calculated through Eq. (9) [1].

$$Q_{cooler,1} = \dot{m}_2(h_2 - h_3) = \dot{m}_{15}(h_{16} - h_{15})$$
$$Q_{cooler,2} = \dot{m}_4(h_4 - h_5) = \dot{m}_{17}(h_{18} - h_{17})$$
$$Q_{heater,1} = \dot{m}_{22}(h_{22} - h_{24}) = \dot{m}_7(h_8 - h_7) \tag{9}$$
$$Q_{heater,2} = \dot{m}_8(h_9 - h_8) = \dot{m}_{25}(h_{25} - h_{26})$$
$$Q_{heater,3} = \dot{m}_{10}(h_{11} - h_{10}) = \dot{m}_{27}(h_{27} - h_{28})$$

where subscripts 4, 5, 7, 8, 9, 10, 11, 17, 18, 22, 24, 27, and 28 refer to the streams shown in Figure (1) [14].

The well-known parameter of the heat exchanger, namely heat exchange effectiveness, can be calculated using Eq (10).

$$\varepsilon_{cooler,1} = \frac{\dot{m}_{15}(h_{15} - h_{16})}{Q_{cooler1,max}} = \frac{\dot{m}_2(h_2 - h_3)}{Q_{cooler1,max}}$$

$$\varepsilon_{cooler,2} = \frac{\dot{m}_{17}(h_{17} - h_{18})}{Q_{cooler2,max}} = \frac{\dot{m}_4(h_4 - h_5)}{Q_{cooler2,max}}$$

$$\varepsilon_{heater,1} = \frac{\dot{m}_7(h_8 - h_7)}{Q_{heater1,max}} = \frac{\dot{m}_{22}(h_{22} - h_{24})}{Q_{heater1,max}} \tag{10}$$

$$\varepsilon_{heater,2} = \frac{\dot{m}_8(h_9 - h_8)}{Q_{heater2,max}} = \frac{\dot{m}_{25}(h_{25} - h_{26})}{Q_{heater2,max}}$$

$$\varepsilon_{heater,3} = \frac{\dot{m}_{10}(h_{11} - h_{10})}{Q_{heater3,max}} = \frac{\dot{m}_{27}(h_{27} - h_{28})}{Q_{heater3,max}}$$

where subscripts 2, 3, 4, 5, 7, 8, 9, 10, 11, 15, 16, 17, 18, 22, 24, 25, 26, 27, and 28 denote the streams depicted in Figure (1) and the subscript max represents the maximum heat exchange occurring in heat exchanger [14].

3.3. Exergy analysis

Exergy is the maximum useful possible work which transforms the system from a specific state to equilibrium with the environment.

The exergy of each stream of the former desired system can be calculated using Eq. (11) [14]:

$$E = \dot{m}[h - h_0 - T(s - s_0)] \tag{11}$$

In Eq. (10), $\dot{m}$ is the mass flow rate of the working fluid, h is the specific enthalpy of the stream, and S is the specific entropy of the stream. h_0 and S_0 are specific enthalpy and entropy in the dead state, respectively.

Exergy analysis is calculated based on the second-law of thermodynamics to identify the source value of thermodynamic inefficiencies.

For each component, exergy of product, ($\dot{E}_P$), as the expected outlet should be calculated. Furthermore, exergy of fuel ($\dot{E}_F$), which is the consumed exergy of the component, is evaluated [20].

The exergy balance can be written as Eq. (12) [14]:

$$\dot{E}_F = \dot{E}_P + \dot{E}_D \tag{12}$$

where ($\dot{E}_D$) is the waste exergy of the component due to irreverssibilities. ($\dot{E}_P$) and ($\dot{E}_F$) of individual subsystems in the previously mentioned cycle are given in Table (2), where E represents exergy of each stream shown in Figure (1).

Table 2. ($\dot{E}_P$) and ($\dot{E}_F$) of individual subsystems

Component	$\dot{E}_P$	$\dot{E}_F$
Compressor 1	E[2]-E[1]	$\dot{w}_{compressor1}$
Compressor 2	E[4]-E[3]	$\dot{w}_{compressor2}$
Cooler 1	E[16]-E[15]	E[2]-E[3]
Cooler 2	E[18]-E[17]	E[4]-E[5]
Throttle valve 1	E[7]	E[6]
Throttle valve 2	E[1]	E[14]
Heater 1	E[8]-E[7]	E[22]-E[24]
Heater 2	E[9]-E[8]	E[25]-E[26]
Heater 3	E[11]-E[10]	E[27]-E[28]
Turbine 1	$\dot{w}_{turbine1}$	E[9]-E[10]
Turbine 2	$\dot{w}_{turbine2}$	E[11]-E[12]

The exergy efficency of each component derived from Eq. (13) [14]:

$$\in_{component} = \frac{\dot{E}_P}{\dot{E}_F} \times 100 \% \tag{13}$$

where $\in$ shows the efficiency of each component.

The relative exergy destruction per component is calculated using Eq. (14) [14]:

$$\in_r = \frac{\dot{E}_{D,r}}{\dot{E}_{D,total}} \times 100 \% \tag{14}$$

where the subscript D denotes destruction and subscript r is calculated according to each component.

In the case of energy storage syatems, it is quite usual to introduce several parameters so as to evaluate the performance of the energy storing system. Commonly, round-trip efficiency is one of these parameters. According to Eq. (15), the mentioned efficiency is defined as the ratio of total output power denoting the capability of electricity generation in the discharge mode by means of turbines to the net input power of the system reflecting the compressor work in the charging mode. Overall, the higher the round-trip efficiency, the less the energy loss in the storage process [15].

$$RTE = \frac{(\dot{w}_{turbine,1} + \dot{w}_{turbine,2})t_{discharge}}{(\dot{w}_{compressor,1} + \dot{w}_{compressor,2})t_{charge}} \quad (15)$$

The exergy efficiency of the whole cycle is calculated as in Eq. (16) [15]:

$$Exergy_{efficiency} = 1 - \left(\frac{Total\ exergy\ destruction}{Inlet\ exergy\ to\ the\ cycle}\right) \quad (16)$$

4. RESULTS AND DISCUSSION

4.1. RESULTS

In order to confirm the validity of the present model, some model components were validated based on the similar data existing in the literature. The data for the purpose of comparison were collected from reference [14]. The obtained results are presented in Table (3).

Table 3. Comparison between the present results and those of Ref. [14]

Component	$\dot{E}_{D,r}$ (kW)	$\dot{E}_{D,r}$ (kW) [14]	Relative error (%)
Compressor	181.4	181.60	0.1101
Turbine	154.6	152.89	1.118
Heat exchanger	254.9	259.10	1.62
Cooler	53.62	53.34	0.525
Throttle valve	47.93	47.94	0.02

The results of the simulation of the proposed cycle are given here. In order to measure the thermodynamic properties of carbon dioxide and Therminol VP-1 oil, a software product called Engineering Equation Solver (EES) is employed. The environment temperature and pressure are set to be 298.15 K and 0.1 MPa for simulation. Mass flow rate of working fluid in the main cycle is considered to be 13.88 kg/s for both charging and discharging cycles. In the present case, charging and discharging periods are both considered to be 6 hours. The main initial parameters of this cycle are listed in Table (4). The initial parameters have been selected so that they can be similar to those of reference [14] in order to make an appropriate comparison between final results.

Table 4. Initial parameters [14]

Parameter	Unit	Value
Ambient temperature	K	298.15
Ambient Pressure	Mpa	0.1
Pressure of high-pressure storage tank	Mpa	20
Pressure of low-pressure storage tank	Mpa	1
Δp of the throttle valve 1	Mpa	0.3
Δp of the throttle valve 2	Mpa	3
Isentropic efficiency of turbines	%	85
Isentropic efficiency of compressors	%	85
Isentropic efficiency of heat exchangers	%	85

Furthermore, conventional exergy analysis has been carried out for this specific system. Thermodynamic properties per state of the proposed cycle are shown in Table (5).

In order to analyze the impact of compressor isentropic efficiency on the performance of the entire cycle, the value of isentropic efficiency of compressors is considered to vary from 80 % to 95 % while other parameters are kept unchanged. Based on Figure (2), upon increasing the efficiency of compressors, both RTE and exergy efficiency values rise as a result of the better performance of compressors.

Table 5. Thermodynamic properties of each state of the cycle

Stream	Working fluid	T (K)	P (MPa)	H (kj/kg)	S ($\frac{kj}{kgK}$)	E (kj/kg)
1	Carbon dioxide	295	0.7	-9.477	-0.3903	1573
2	Carbon dioxide	443.9	3.74	117.6	-0.3465	3288
3	Carbon dioxide	313.2	3.72	-23.36	-0.7229	2813
4	Carbon dioxide	474.9	19.87	93.85	-0.6854	4407
5	Carbon dioxide	313.2	19.85	-229.6	-1.539	3271
6	Carbon dioxide	313.2	19.85	-229.6	-1.539	3271
7	Carbon dioxide	311.4	16.85	-229.6	-1.527	3218
8	Carbon dioxide	420.2	16.83	26.46	-0.8104	3941
9	Carbon dioxide	620.2	16.81	284	-0.3053	5605
10	Carbon dioxide	476.4	4.08	150.6	-0.2904	3540
11	Carbon dioxide	628.6	4.06	315.5	0.01233	4711
12	Carbon dioxide	491.4	0.9855	176.9	0.0274	2551
13	Carbon dioxide	298.2	0.9655	-9.297	-0.4479	1826
14	Carbon dioxide	298.2	0.9655	-9.297	-0.4479	1826
15	Water	298.2	1	105.7	0.3667	1.574

| 16 | Water | 422 | 1 | 627.8 | 1.83 | 396.5 |
17	Water	298.2	1	105.7	0.3667	2.962
18	Water	448.4	1	742.3	2.093	1037
19	Water	439.3	1	702.6	2.004	1427
20	Water	298.2	1	105.7	0.3667	4.536
21	Water	439.3	1	702.6	2.004	1427
22	Water	439.4	1.3	703	2.004	1431
23	Water	298.2	0.98	105.7	0.3667	4.303
24	Water	362.2	1	373.9	1.181	375.6
25	Therminol VP-1 oil	655.5	0.1	754.7	1.638	4934
26	Therminol VP-1 oil	564.7	0.1	535.1	1.278	2910
27	Therminol VP-1 oil	655.5	0.1	754.7	1.638	3179
28	Therminol VP-1 oil	564.7	0.1	535.1	1.278	1875
29	Therminol VP-1 oil	564.7	0.1	535.1	1.278	4785
30	Therminol VP-1 oil	655.5	0.1	754.7	1.638	8114
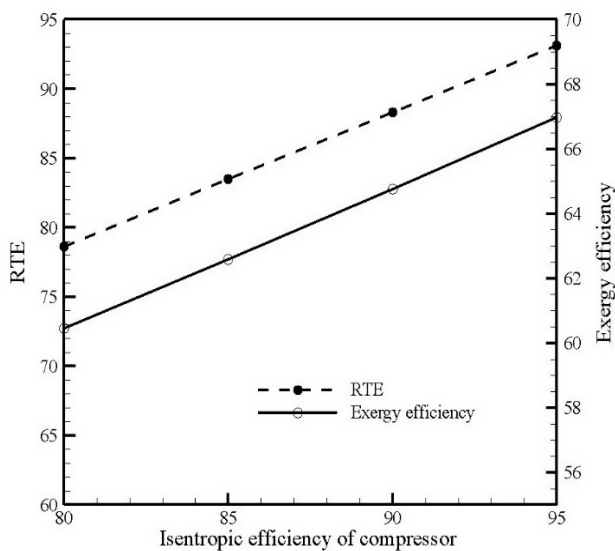
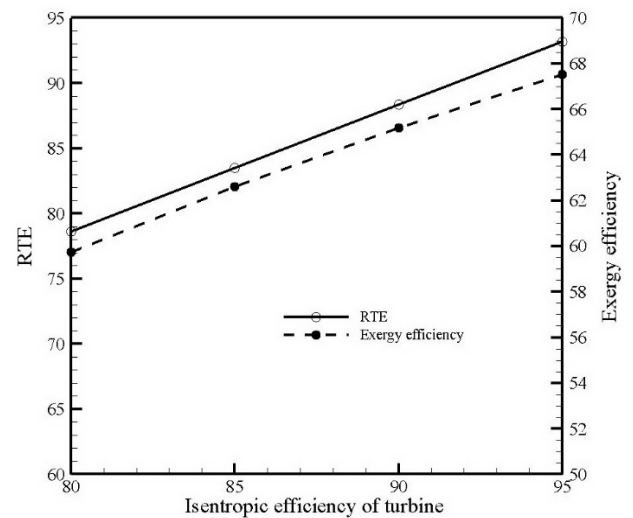**Figure 2.** Impact of isentropic efficiency of compressors on the cycle performance

Figure 3. Impact of isentropic efficiency of turbines on the cycle performance

In a similar manner, the impact of changes in the turbine isentropic efficiency on RTE and exergy efficiency is presented in Figure (3).

By the same token, upon improving the performance of turbines, RTE and exergy efficiency increase.

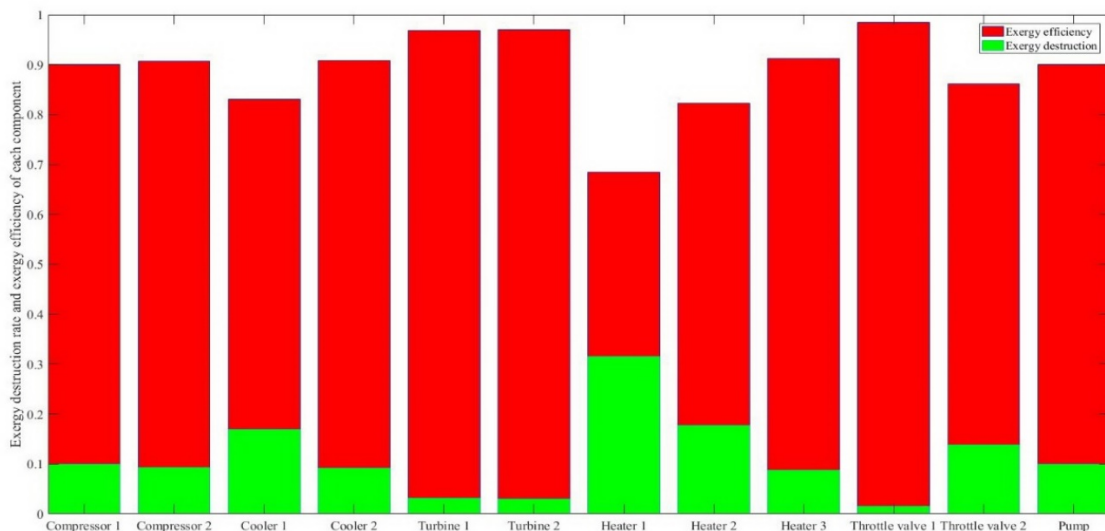Figure (4) presents the exergy destruction and exergy efficiency of each constituent of the entire system.

Figure 4. Comparison between exergy efficiency and exergy destruction of individual components

Moreover, the relative exergy destruction percentage of individual components is given in Figure (5).
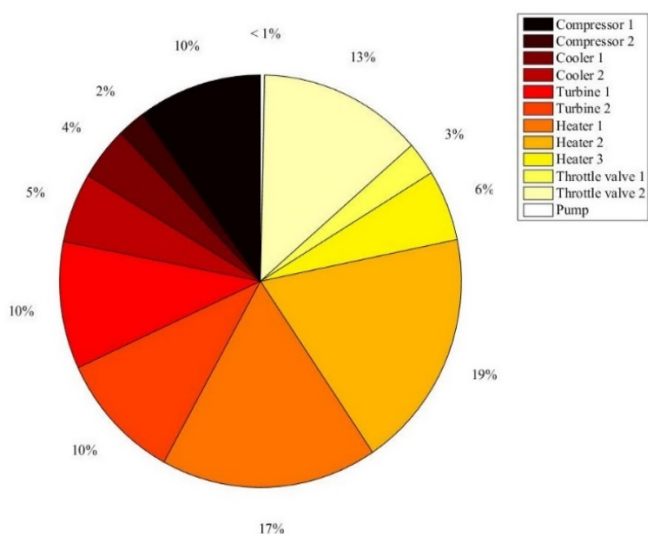

Figure 5. Relative exergy percentage of individual components

From the above stated results, Heater 2 and pump have the largest and smallest shares of relative exergy destruction, respectively. Most of the constituents represent high exergy efficiency (more than 80 %) except Heater 1, which is 68.42 %. Of note, Heater 1 uses hot water from the hot water storage tank to recover it in the cycle and the temperature of carbon dioxide increases from 311.4 K to 420.2 K. This increase is greater through Heater 2 and Heater 3 due to the higher thermal capacity of Therminol VP-1 than water.

In this paper, a Parabolic Trough Collector (PTC) was suggested as a resource for the system to enhance the cycle performance. As was mentioned formerly in this paper, the principal drawback of renewable sources is their instability and fluctuating nature. In order to cope with this trouble, thermal storage tanks have been designed to balance the required energy.

In this study, System Advisor Model (SAM) version 2020.2.29 developed by the National Renewable Energy Lab (NREL) was employed to design a parabolic trough collector. To this end, SAM software was utilized due to its user-friendly environment, its open-source platform, and up-to-date meteorological data available. It is also a well-known software product for designing both performance and financial model.

The principal design parameters of the suggested parabolic through collector due to SAM database is given in Table (6).

In order to initialize the simulation, meteorological data are to be added to the software. The required data for this paper are downloaded from the website "nsrdb.nrel.gov" with station ID2697736.

Table 6. Design parameters of PTC

DNI	$950 \frac{W}{m^2}$
HTF hot temperature	664.15 K
Hours of storage	6 h

The meteorological data utilized in this study originate from Kerman province located in Iran at latitude of 30.29 and longitude of 57.06. The exact date on 06/22/2019 is determined as the typical day for simulating the operation of the aforementioned system.

Figure (6) presents the Direct Normal Incidence (DNI) on the surface and dry bulb temperature with respect to the aforesaid day.
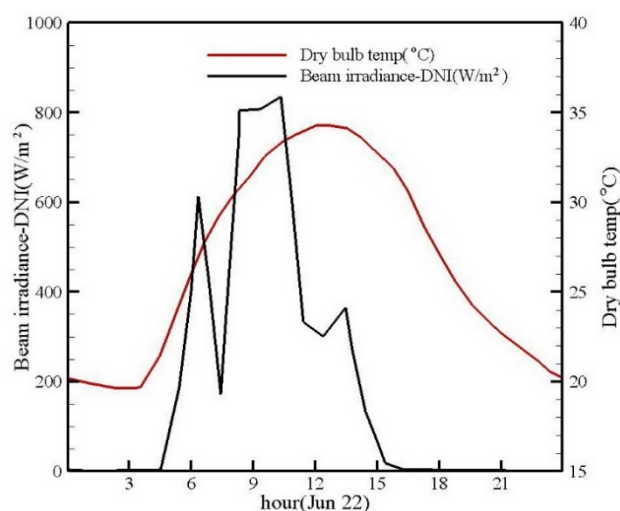

Figure 6. DNI and dry bulb temperature of the selected day (6/22/2019)

According to Figure (6), the dry bulb temperature increases within the time interval starting at 5:00 in the morning to around 14:00 in the afternoon. Furthermore, DNI profile presents that the solar field has the potential to supply sufficient heat in the discharge mode when the sun goes down.

System design, solar field, collector, receiver, and thermal storage parameters, as shown in Table (7), should be fed to the SAM software first.

Table 7. Characteristics of PTC

Characteristics	Value
Total plant capacity	111 MWe
Total land area	1.4 × (solar field area) m²
Collectors and solar field	
Collector type	Skye fuel sky through
Number of loops	181
Single loop aperture	5248 m²
Solar multiple	2
Water usage per wash	$0.7 \frac{L}{m^2}$ aperture
Row spacing	15
Thermal receiver and HTF properties	

Receiver type	Schott PTR80
Absorber tube inner diameter	0.076 m
Absorber tube outer diameter	0.08 m
Glass envelope inner diameter	0.115 m
Glass envelope outer diameter	0.12 m
Absorber material type	304 L
HTF type	Therminol VP-1
Design loop outlet temperature	391 ℃
Design loop inlet temperature	293 ℃
Boiler operating pressure	100 bar
Thermal energy storage	
Full load hours of TES	6 h
Storage type	Two tanks
Storage fluid	Therminol VP-1
Tank diameter	65.026 m
Tank height	12 m
Tank loss coefficient	$0.4 \ ^W/_{m^2K}$
Estimated heat loss	1.38695 MWt

Afterwards, the temperature inside the storage tanks, mass flow rate of the working fluid and further cycle properties can be modeled using SAM software.

Amongst the various heat transfer fluids, Therminol VP-1 is considered to be a suitable choice due to its high specific heat capacity [17]. The hot Therminol VP-1 temperature profile in the hot storage tank is depicted in Figure (7).
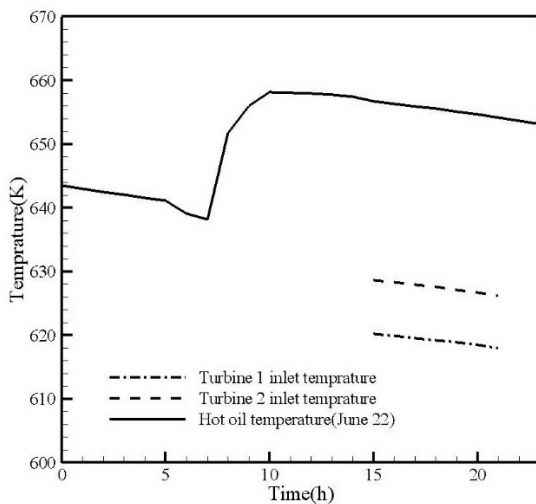

Figure 7. Hot oil temperature profile for the hot storage tank

According to Figure (7), from the early hours in the morning to the noon, the temperature of the oil in hot storage tank increases due to sunshine. Then, in the afternoon from 15:00 to 21:00 in the evening when available sunshine dims, the temperature of hot oil lessens as a result of heat dissipation to the environment.

In this paper, it is considered that the system starts to discharge in the time range of 15:00 to 21:00 for 6 full hours. The turbine inlet temperature plays an important role in the cycle performance. In order to investigate this impact, the inlet temperature changes for Turbines 1 and 2 are shown in Figure (7). Subsequently, based on the whole performance of the system in the discharge mode is presented in Figure (8).

Based on Figures (7) and (8), from 15:00 to 21:00, the temperature of hot oil and the inlet temperature of turbines are reduced simultaneously. Therefore, the RTE decreases from 93.14 % to 92.74 %. In the same manner, the exergy efficiency lessens from 66.98 % to 66.72 %. This slight difference in efficiencies through time represents that the sun fluctuations during the day have a minor effect on the functionality of the system due to role of storage tanks.
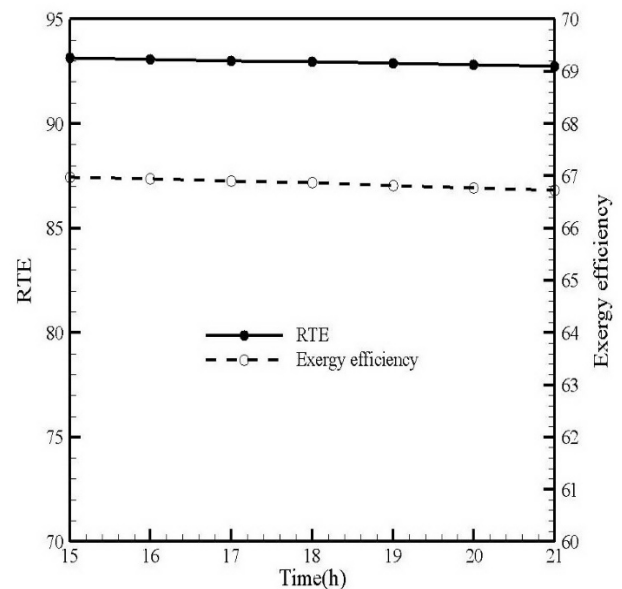

Figure 8. Performance analysis of the system in the discharge mode

In order to demonstrate the capability of the present modeling, a comparison between the present results and similar work done by Liu [14] was made.

Table 8. Comparison in exergy efficiency obtained in the present study and reference [14]

	Present study	**Liu [14]**
Exergy efficiency (%)	66.98	59

As it is obvious from Table (8), the exergy efficiency of the present study model is higher than that of the reference.

5. CONCLUSIONS

This paper presented the integration between compressed carbon dioxide energy storage and parabolic trough collector. Furthermore, energy and exergy analyses were conducted for every individual constituent. Moreover, the fluctuating nature of the sun in parabolic trough collector in the discharging mode was taken into account on an hourly basis, from 15:00 to 21:00. The principal concluding remarks can be addressed as follows:

-Exergy efficiency and round-trip efficiency of the system for a random day (22 June/2019) at 15:00 was reported to be 66.98 % and 93.14 %, respectively, being higher than the previous data reported in the literature [14].

-All the components had high exergy efficiency above 80 % except Heater 1 with an exergy efficiency rate of 68.42 %.

-After a while, throughout the discharging period, the inlet temperatures of both Turbines 1 and 2 decreased and exergy efficiency and round-trip efficiency were reduced.

6. ACKNOWLEDGEMENT

The authors gratefully acknowledge the editor and reviewers for their contribution to completing this manuscript.

NOMENCLATURE

C_p	Specific heat capacity (Kj/Kg.K)
E	Exergy flow rate (KW)
h	Specific enthalpy (Kj/Kg)
ṁ	Mass flow rate (Kg/s)
P	Pressure (MPa)
Q	Heat flow rate (KW)
S	Entropy (Kj/Kg.K)
T	Temperature (K)
t	Time (s)
W	Power (KW)
Greek letters	
η	Efficiency (%)
Subscripts	
0	Dead state
c	Compressor
D	Destruction
F	Fuel
HST	High Pressure Storage Tank
is	isentropic
LST	Low Pressure Storage Tank
max	Maximum
P	Product
t	Turbine
Abbreviations	
A-CAES	Adiabatic CAES
CAES	Compressed Air Energy Storage
CR	Cooler
D-CAES	Diabatic CAES
DNI	Direct Normal Incidence
EES	Engineering Equation Solver
EVR	Energy Generated per Unit Volume
Eq.	Equation
HTF	Heat Transfer Fluid
GWP	Global Warming Potential
LAES	Liquid Air Energy Storage
NREL	National Renewable Energy Lab
ODP	Ozone Depleting Potential
PHES	Pumped Hydro Energy Storage
RTE	Round-Trip Efficiency
SAM	System Advisor Model

REFERENCES

1. Zhang, Y., Yao, E., Zhang, X. and Yang, K., "Thermodynamic analysis of a novel compressed carbon dioxide energy storage system with low-temperature thermal storage", *International Journal of Energy Research*, Vol. 44, No. 8, (2020), 6531-6554. (https://doi.org/10.1002/er.5387).

2. Rehman, S., Al-Hadhrami, L. and Alam, M., "Pumped hydro energy storage system: A technological review", *Renewable and Sustainable Energy Reviews*, Vol. 44, (2015), 586-598. (https://doi.org/10.1016/j.rser.2014.12.040).

3. Wang, M., Zhao, P., Wu, Y. and Dai, Y., "Performance analysis of a novel energy storage system based on liquid carbon dioxide", *Applied Thermal Engineering*, Vol. 91, (2015), 812-823. (https://doi.org/10.1016/j.applthermaleng..08.081).

4. (https://patents.google.com/patent/US2433896A/en).

5. Zhou, Q., Du, D., Lu, C., He, Q. and Liu, W., "A review of thermal energy storage in compressed air energy storage system", *Energy*, Vol. 188, (2019). (https://doi.org/10.1016/j.energy.2019.115993).

6. Kere, A., Goetz, V., Py, X., Olives, R., Sadiki, N. and Mercier, E., "Dynamic behavior of a sensible-heat based thermal energy storage", *Energy Procedia*, Vol. 49, (2014), 830-839. (https://doi.org/10.1016/j.egypro.2014.03.090).

7. Guizzi, G.L., Manno, M., Tolomei, L.M. and Vitali, R.M., "Thermodynamic analysis of a liquid air energy storage system", *Energy*, Vol. 93, No. 1977, (2015) 1639-1647. (https://doi.org/10.1016/j.energy.2015.10.030).

8. Baxter, J.W. and Bumby, J.R., "Fuzzy control of a mobil robotic vehicle", *Proceedings of the Institution of Mechanical Engineers, Part I : Journal of Systems and Control Engineering*, Vol. 209, No. 2, (1995). (https://doi.org/10.1243/PIME_PROC_1995_209_369_02).

9. Chen, H., Goswami, D.Y. and Stefanakos, E.K., "A review of thermodynamic cycles and working fluids for the conversion of low-grade heat", *Renewable and Sustainable Energy Reviews*, Vol. 14, No. 9, (2010), 3059-3067. (https://doi.org/10.1016/j.rser.2010.07.006).

10. Rony, R.U., Yang, H., Krishnan, S. and Song, J., "Recent advances in transcritical CO_2 (R744) heat pump system: A review", *Energies*, Vol. 12, No. 3, (2019). (https://doi.org/10.3390/en12030457).

11. Alami, A.H., Hawili, A., Hassan, R., Al-Hemyari, M. and Aokal, K., "Experimental study of carbon dioxide as working fluid in a closed-loop compressed gas energy storage system", *Renewable Energy*, Vol. 134, (2019), 603-611. (https://doi.org/10.1016/j.renene.2018.11.046).

12. Mercangöz, M., Hemrle, J., Kaufmann, L., Z'Graggen, A. and Ohler, C., "Electrothermal energy storage with transcritical CO_2 cycles", *Energy*, Vol. 45, No. 1, (2012), 407-415. (https://doi.org/10.1016/j.energy.2012.03.013).

13. Liu, H., He, Q., Borgia, A., Pan, L., and Oldenburg, C.M., "Thermodynamic analysis of a compressed carbon dioxide energy storage system using two saline aquifers at different depths as storage reservoirs", *Energy Conversion and Management*, Vol. 127, (2016), 149-159. (https://doi.org/10.1016/j.enconman.2016.08.096).

14. Liu, Z., Liu, B., Guo, J., Xin, X. and Yang, X., "Conventional and advanced exergy analysis of a novel transcritical compressed carbon dioxide energy storage system", *Energy Conversion and Management*, Vol. 198, No. July, (2019), 111807. (https://doi.org/10.1016/j.enconman.2019.111807).

15. Zhang, Y., Yang, K., Hong, H., Zhong, X. and Xu, J., "Thermodynamic analysis of a novel energy storage system with carbon dioxide as working fluid", *Renewable Energy*, Vol. 99, (2016), 682-697. (https://doi.org/10.1016/j.renene.2016.07.048).

16. Bishoyi, D. and Sudhakar, K., "Modeling and performance simulation of 100 MW LFR based solar thermal power plant in Udaipur India", *Resource-Efficient Technologies*, Vol. 3, No. 4, (2017), 365-377. (https://doi.org/10.1016/j.reffit.2017.02.002).

17. Zhang, Y., Liang, T., Yang, C., Zhang, X. and Yang, K., "Advanced exergy analysis of an integrated energy storage system based on transcritical CO_2 energy storage and Organic Rankine Cycle", *Energy Conversion and Management*, Vol. 216, No. April, (2020), 112938. (https://doi.org/10.1016/j.enconman.2020.112938).

18. Zhang, Y. and Yao, E., "Comparative analysis of compressed carbon dioxide energy storage system and compressed air energy storage system under low-temperature conditions based on conventional and advanced exergy methods", *Journal of Energy Storage*, Vol. 35, No. October 2020, (2021). (https://doi.org/10.1016/j.est.2021.102274).

19. Zhang, Y., Yao, E., Tian, Z., Gao, W. and Yang, K., "Exergy destruction analysis of a low-temperature compressed carbon dioxide energy storage system based on conventional and advanced exergy methods", *Applied Thermal Engineering*, Vol. 185, No. August 2020, (2021), 116421. (https://doi.org/10.1016/j.applthermaleng.2020.116421).

20. Kreith, F., "CRC Handbook of Thermal Engineering", **Cycle**, (2000), (https://www.springer.com/gp/book/9783540663492).